Dalton Transactions

Accepted Manuscript

ROYAL SOCIETY OF CHEMISTRY

www.rsc.org/dalton

Journal Name

RSCPublishing

ARTICLE

Silane-coated magnetic nanoparticles with surface thiol functions for conjugation with gold nanostars

Cite this: DOI: 10.1039/xoxxoooooox

Piersandro Pallavicini,*[a] Elisa Cabrini,[a] Alberto Casu,[b] Giacomo Dacarro,[a] Yuri Diaz-Fernandez,[c] Andrea Falqui,[b] Chiara Milanese[a] and Francesco Vita,[d]

Received ooth January 2012,
Accepted ooth January 2012

DOI: 10.1039/xoxxoooooox

www.rsc.org/

Small (d ~ 8 nm) magnetite nanoparticles, Fe_3O_4NP, are prepared and coated with mercaptopropyl trimethoxysilane (MPTS) to form Fe_3O_4NP@MPTS. In the coating step controlled MPTS/Fe_3O_4NP molar ratios are used, ranging from 1 to 7.8×10^4. The total quantity of MPTS per Fe_3O_4NP is determined by SEM-EDS analysis and the average number of free, reactive –SH groups per Fe_3O_4NP is calculated by a colorimetric method. At very low molar ratios MPTS forms a submonolayer on the Fe_3O_4NP surface with all –SH free to react, while on increasing the MPTS/Fe_3O_4NP molar ratio the $(CH_3O)_3$Si- groups of MPTS polymerize, forming a progressively thicker shell, in which only a small fraction of the –SH groups, positioned on the shell surface, is available for further reaction. The MPTS shell reduces the magnetic interactions occurring between the magnetite cores, effectively preventing the occurrence of collective magnetic states, with Fe_3O_4NP@MPTS showing the typical behaviour expected for a sample with a mono-modal size distribution of superparamagnetic nanoparticles. Interaction of Fe_3O_4NP@MPTS with gold nanostars (GNS) was tested, using both Fe_3O_4NP@MPTS with a MPTS submonolayer and with increasing shell thickness. Provided that a good balance is used between the number of available –SH and the overall size of Fe_3O_4NP@MPTS, the free thiols of such nanoparticles bind GNS decorating their surface, as shown by UV-Vis spectroscopy and TEM imaging.

Introduction

Iron oxides magnetic nanoparticles are intensely studied as they find applications in many areas, especially in biology and medicine, e.g. in magnetic resonance as imaging contrast agents,[1] in diagnostics,[2] in magnetic cell separation and purification,[3] in anti-tumoral therapies as drug carriers and in magnetic-generated hyperthermal therapies.[4,5] The surface of iron oxides magnetic nanoparticles must be coated in order to enhance their stability against aggregation and to prolong storage time. Moreover, if the iron oxides magnetic nanoparticles are intended for in-vitro or in-vivo use, the coating must be biocompatible and, in many cases, it should also allow conjugation with biomolecules. Stabil
izers such as citrate,[6] sodium oleate[7] and polyethylene glycols[7] have been used. The drawback of such coatings is the lability and low strength of the bond between surface and coater, based on the coordinative Fe^{n+}-carboxylate and Fe^{n+}-ether interaction. As an alternative, alkyl phosphonates have been used,[8-10] with the chelate R-P-$(O\text{-}Fe)_2$ moiety increasing their stability and the Fe-O-P bonds described as "covalent" (although this statement is still under debate).[11] Based on similar interactions, also siloxane coatings have been employed. In this case, surface grafting is within a similar frame as for the grafting chemistry of siloxanes on silica.[12] The formation of one, two or three Si-O-Fe bonds from the same Si centre may be hypothesized, as sketched in Figure 1 A-C, respectively, for the case of MPTS. In cases B anc C, the Si-O- groups may be connected with a vicinal, surface-grafted silane or bind further MPTS molecules leading to lateral and vertical polymerization, as sketched in Figure 1D. Trialkoxysiloxanes $(RO)_3$Si-$(CH_2)_n$-X are commercially available, with an arsenal of X functions and a typical n value of 3. MPTS,[13,14] aminopropyltrimethoxy silane[15,16] and 3-glycidoxypropyltrimethoxylsilane[13] have been used for coating iron oxides magnetic nanoparticles, due to the possibility offered by their terminal functions to undergo further chemistry and modify the coating layer. Iron oxides magnetic nanoparticles bearing such silanes on the surface have been conjugated with bio-interesting molecules such as trypsin,[13] oligonucleotides,[17,18] DNA,[19,20] enzymes,[21] and antibodies.[22,23] As it has been recently reviewed,[24,25]

conjugation of iron oxides magnetic nanoparticles with gold in hybrid nanoparticles is also a matter of interest for their possible theranostic applications. The typical approach leads to core-shell structures, consisting of a core of magnetic iron oxides on which small gold nanoparticles adhere and in a further step form a continuous spherical shell.[26-28]

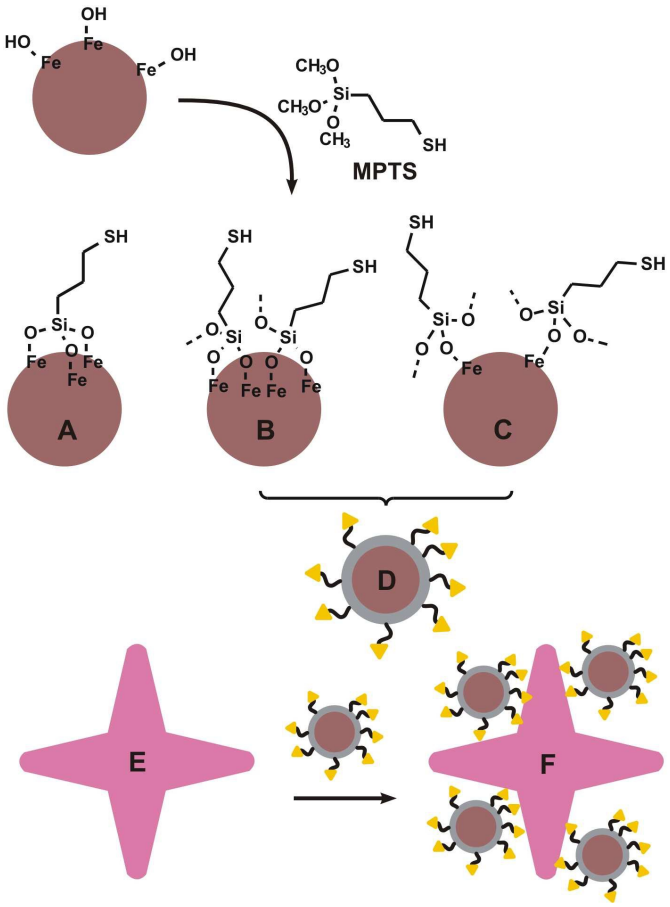

Fig 1 Schematic representation of the possible modalities of surface functionalization by MPTS of iron oxides magnetic nanoparticles (including the Fe_3O_4NP descibed in this paper) (A-C); E: schematic representation of the interaction of Fe_3O_4NP@MPTS with GNS

An example of the reverse approach, i.e. gold nanorods decorated on the surface with iron oxides magnetic nanoparticles, has also been reported,[29] with these hybrids capable of simultaneous optical detection based on Au plasmonic properties, magnetic separation, and photothermal necrosis of multiple bacterial strains. We are working on the synthesis and biomedical applications of GNS, i.e. gold nanoparticles featuring a core and from 2 to 6 branches protruding from it (sketch in Figure 1E).[30-32] These are relatively large nanoparticles, with tip-to-tip distance ranging from 50 to 70 nm depending on the synthetic conditions, that are prepared with wet synthesis in a seed-growth approach, using laurylsulphobetaine (LSB) as the protecting and directing agent. LSB is a zwitterionic surfactant weakly bound to the gold surface, easy to be removed and allowing facile surface grafting of thiolated molecules.[33-34] These GNS display efficient photothermal conversion when irradiated on their Near-IR localized surface plasmon resonance (LSPR)[35] demonstrating antibiofilm activity.[36] With the aim of preparing GNS-iron oxides magnetic nanoparticles hybrids, i.e. larger GNS decorated with small nanopartiocles of magnetic iron oxides, see Figure 1F, in this paper we present the synthesis of Fe_3O_4NP. These are superparamagnetic magnetite nanoparticles, that we further coat with MPTS to obtain Fe_3O_4NP@MPTS. Our approach allows the controlled formation of a MPTS shell around the Fe_3O_4NP core, as in Figure 1D, with a tunable overall quantity of grafted MPTS and a tunable number of available -SH groups on the shell surface. The influence of the MPTS coating on the magnetic properties of the two systems was also studied, indicating how it contributes in lowering the effect of the magnetic interactions among the coated particles if compared with those not coated. Finally The available –SH functions have been used both to conjugate the coated Fe_3O_4NP with stabilizing polyethileneglycol chains and to make them interact with the Au surface of GNS, demonstrating that it is possible to obtain efficient decoration of the latter. These hybrids are a novelty that may have interesting applications eg in thermal therapies in nanomedicine area[37], as both their photothermal[35,36] and magnetothermal[35] properties can be used separately or simultaneously, obtaining multilevel controlled heating on the nanoscale[38].

Experimental

Materials.

Iron(II) chloride tetrahydrate ($FeCl_2 \cdot 4H_2O$) > 99%, Iron(III) chloride hexahydrate ($FeCl_3 \cdot 6H_2O$) > 99%, perchloric acid (60% in water), chloridric acid (37% in water), (3-mercaptopropyl)trimethoxy silane (MPTS) 95%, ethanol, acetone, silve nitrate, sodium borohydride, tetrachloroauric acid, laurylsulphobetaine, ascorbic acid, Tetramethylrhodamine-5-maleimide (RHM) > 85%, Methoxypolyethylene glycol maleimide (PEG-MAL) > 90% (mw 5000) were all purchased from Sigma-Aldrich and used as such.

Syntheses.

Fe_3O_4 nanoparticles (Fe_3O_4NP). The synthesis is a modification of the procedure published by Massart.[39] In a typical preparation, 1.08 g (4.00 mmol) $FeCl_3 \cdot 6H_2O$ were dissolved in 4.0 mL bidistilled water. Separately, 0.39 g (1.96 mmol) $FeCl_2 \cdot 4H_2O$ were dissolved in 2.0 mL bidistilled water. In a 250 mL beaker 2.22 mL of ammonia (37% in water) were diluted to 50 mL (final concentration ~ 0.70 M). To this solution the Fe(III) and Fe(II) solutions are added in a fast sequence, and the beaker is mildly hand shaken until the solution takes a black color. The nanoparticles are magnetically separated on the bottom of the beaker, the supernatant is discarded and the Fe_3O_4NP slurry is treated with 50 mL $HClO_4$ 2.0M. The sample is then centrifuged (10 minutes, 4000 rpm, 1500g), the supernatant is discarded and the pellet is redissolved in 50 mL bidistilled water. The preparation does not

require the use of a N_2 atmosphere. This colloidal solution is stable for 15 days. Separation of a solid sample of Fe_3O_4NP can be easily attained by addition of a 10-fold volume of acetone, decantation and drying under N_2 flux.

Fe_3O_4@MPTS nanoparticles. In a typical preparation, 10 mL bidistilled water, 20 mL ethanol and 1.0 mL of Fe_3O_4NP aqueous solution are mixed at room temperature in a round flask. The solution is stirred with a mechanical stirrer to avoid separation of the Fe_3O_4NP in case of the use of a magnetic one. The solution is made slightly basic (pH 8-9) by addition of 37 % aqueous ammonia. 10μL (5.38×10^{-5} mol) MPTS (d=1.057 g/mL) are then added and the reaction is stirred for further 3.5 hours at room temperature in the stoppered flask. The product is purified by ultracentrifugation (10 min, 6000 rpm, 3380 g), discarding of the supernatant and redissolution of the pellet in 20mL of bidistilled water (the cycle is repeated two times). In order to tune the quantity of –SH on the nanoparticles surface, we used 1, 2.5 and 5.0 mL of the Fe_3O_4NP solution with 10, 20 or 30 μL of pure MPTS (for large MPTS/Fe_3O_4NP ratios) or 50-500 μL of a 10^{-4}M MPTS solution in ethanol.

Fe_3O_4@MPTS-PEG nanoparticles. To 5.0 mL of an aqueous solution of Fe_3O_4NP@MPTS (prepared with 30 μL of MPTS) we added 30, 25 or 15 μL of PEG_{5000}-maleimide in a stoppered vial. The reaction was kept at 40 °C for 16 h on a reciprocating stirrer. The colloidal solution was then centrifuged at 13000 rpm (15870 g) and the pellet redissolved in 5.0 mL bidistilled water by sonication. The centrifugation/redissolution procedure was repeated, to guarantee complete separation of untreated PEG-MAL.

Gold nanostars (GNS). GNS were prepared as described.[30,31] In brief: the seed solution is prepared as follows: 5mL of $HAuCl_4$ 5×10^{-4}M in water are added to 5mL of an aqueous solution of LSB 0.2M. The solution was gently stirred and 0.6mL of a previously ice-cooled solution of $NaBH_4$ 0.01M in water were added. A 12μL volume of the obtained spherical gold seeds (5nm in diameter) were added under stirring to a Growth solution was prepared as follows: 180uL $AgNO_3$ 0.004M, 5.0mL $HAuCl_4$ 0.001 M and 85μL ascorbic acid 0.0788M were added in this order to 5.0 mL of a 0.2 M LSB solution. Finally, a 12μL volume of the obtained spherical gold seeds (5nm in diameter) was added under stirring to the growth solution. Under these conditions, GNS has their main LSPR absorption (LSPR = localized surface plasmon resonance) at ~ 800 nm and a less intense LSPR at ~ 630 nm, concentration of Au is 0.0591 g/L corresponding to a GNS concentration of 1.96×10^{-9} M.

[Fe_3O_4NP@MPTS]@GNS. 10 mL of GNS solution in bidistilled water (1.96×10^{-11} mol) were treated with 10-200 μL volumes of freshly prepared Fe_3O_4NP@MPTS solution. UV-Vis absorption spectra were recorded at each addition, after 10 minutes equilibration time. Spectra taken on the same solutions after further 30 minutes showed no difference. Samples for Transmission Electron Microscopy (TEM) imaging were prepared using GNS solutions within 1 hour from Fe_3O_4NP@MPTS addition, diluting 1 mL to 20 mL in bidistilled water and dropcasting 10 μL of the diluted solution on the grid.

Methods.

Optical determination of free thiols on Fe_3O_4NP@MPTS. 100 μL of a 10^{-3} M aqueous RHM solution were added to 5.0 mL of Fe_3O_4NP@MPTS solution. The solution was allowed to react for 15 h at room temperature, in the dark, on a reciprocating stirrer. The solution was then ultracentrifuged at 13000 rpm (15870 g) for 10 min, the supernatant discarded and the pellet redissolved in 5.0 mL bidistilled water. The centrifugation, separation and redissolution procedure was repeated a second time to eliminate all unreacted RHM. The UV-Vis absorption spectrum of the nanoparticles solution is recorded. The solution absorbance at 559 nm is used to determine the concentration of RHM grafted to Fe_3O_4NP@MPTS by the Lamber-Beer law, using the molar extinction coefficient of RHM in water at 550 nm (ε_{550} = 82000 $M^{-1}cm^{-1}$).[40]

ICP-OES analysis. Fe_3O_4NP samples were prepared treating 1 mL of the colloidal solution with 5 mL diluted aqua regia (2mL aqua regia + 3mL water). Fe_3O_4NP@MPTS samples were prepared by direct treatment of the centrifugate pellet with 5mL diluted aqua regia (2mL aqua regia + 3mL water). The solutions were analysed with a Perkin Elmer ICPOES OPTIMA3000 instrument.

Uv-VIS spectroscopy. Spectra were taken on an Agilent Cary60 UV-Vis instrument, using 1 cm glass cuvettes.

DLS and Pz (zeta potential). DLS experiments and Z-potential determination were performed on a Malvern Nano ZS90 instrument, with a 1 cm glass cuvette and a dedicated Malvern immersion device for Pz.

X-ray diffraction. About 5 mg of powder were deposited on a Silicon zero background sample holder by Bruker and the X-ray diffraction patterns were obtained using a Bruker D5005 instrument equipped with Bragg-Brentano geometry, a cathodic source of Cu (1.54 Å, 30 kV, 40 mA) and a Position Sensitive Detector PSD ASA-S from MBraun by counting 10 sec for each 0.02 ° angular step in the 2theta range from 20 ° to 80°.

Transmission Electron Microscopy (TEM). TEM images od Fe_3O_4NP and Fe_3O_4NP@GNS were taken on a JEOL JEM-1200 EX II 140 instrument, using 100-fold diluted solutions with bidistilled water. 10 μL were deposited on nickel grids (300 mesh) covered with a Parlodion membrane and allowed to dry in a desiccator. The diameter of the nanoparticles was calculated using the ImageJ software (http://imagej.nih.gov/ij/). TEM images of GNS decorated with Fe_3O_4NP@MPTS were obtained on a FEI Tecnai T20 instrument instrument, after a 20-fold dilution with bidistilled water, dropcasting 10 μL of solution on nickel grids (300 mesh) covered with a Parlodion membrane and allowed to dry in a dessicator.

Scanning Electron Microscopy (SEM) + Energy Dispersion Spectroscopy (EDS). Scanning electron microscopy images were taken using an EvoMA10 (Zeiss, Germany) microscope equipped with a LaB_6 filament. The elemental composition of the samples was determined by Energy-dispersive X-ray spectroscopy using an INCA Energy 350 X Max detector from

Oxford Instruments, equipped with a Be window. Cobalt standard was used for the calibration of the quantitative elementary analysis.

Thermogravimetric Analysis (TGA). Thermogravimetric analyses were performed in a Q2000 instrument by TA Instruments (USA) by heating about 5 mg of sample in a Pt sample holder from room temperature to 800 °C at 10°C/min under Ar flux.

Fourier Transform Infrared Spectroscopy (FT-IR) analysis. The FT-IR spectra were collected in attenuated total reflection in transmittance mode using NICOLET iS10 instrument, THERMO SCIENTIFIC. Data acquisition was performed in 256 scans with spacing of 0.482 cm^{-1}. For every sample a background (FT-IR spectrum for empty sample holder) was acquired and subtracted from the FT-IR spectrum of the sample obtained in the same conditions.

Magnetic characterization. The samples magnetic behaviour was studied by determining how their magnetization depended on both the temperature, keeping constant the external magnetic field, and on the external magnetic field, keeping constant the temperature. All the measurements were performed by a Quantum Design MPMS-7XL SQUID magnetometer, equipped with a superconducting magnet capable to produce fields in the ±70 kOe range, and temperatures from 1.9 to 400 K. Zero-field-cooled (ZFC) magnetization curves were measured by cooling samples in zero magnetic field down to 5K and then by increasing the temperature up to 400 K under an applied field of 25 Oe, while the Field-cooled (FC) curves were recorded by cooling the samples in the same field and thermal range. Thermoremanent magnetizations (TRM) were then measured by heating again the samples after having set to zero the magnetic field. The field dependence of the samples magnetization (isothermal hysteresis loop) was recorded in the ±70 kOe range, at T=5 K.

Results and discussion

1. Fe_3O_4NP. The preparation of Fe_3O_4NP is a modified version of the classic preparation described by Massart[39] in 1981.

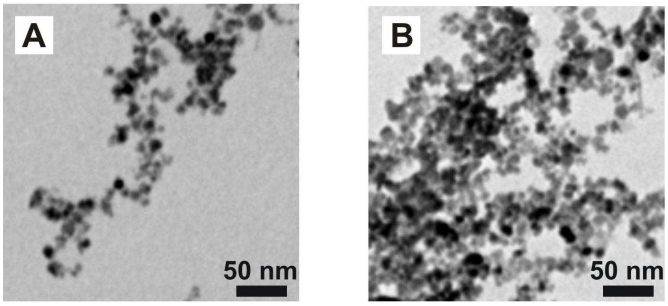

Fig 2 A: TEM image of Fe_3O_4NP (detail of a larger image reproduced in ESI, S1.1); **B**: TEM image of Fe_3O_4NP@MPTS (detail of a larger image reproduced in ESI, S2.1)

We use 10-fold smaller volumes with respect to the original preparation, in order to obtain a volume of product suitable to be subdivided in small ultracentrifuge tubes (10 mL each). The chlorides of Fe(II) and Fe(III) are dissolved in pure water instead of in 2M HCl and mixed in a 1:2 molar ratio in an aqueous solution made basic with 0.7 M NH_3. Gently handshaking leads to the immediate formation of black - dark brown Fe_3O_4 magnetite nanoparticles. These can be decanted from the supernatant using a magnet at the bottom of the beaker. The slurry is then treated with 2M $HClO_4$ to obtain a solution that is ultracentrifuged. The obtained pellet is redissolved in bidistilled water, using the same volume as that used for ultracentrifugation (10 mL). This is the product used for characterization and further surface functionalization. A 61% yield was calculated with ICP-OES, by determining the total concentration of Fe (Fe_{TOT}) in the Fe_3O_4NP solution, compared with the Fe(II) + Fe(III) starting concentration. DLS measurements revealed a 17 nm (σ = 3 nm) diameter. The surface charge is positive, with Pz = + 28 mV (σ = 1 mV). However, TEM imaging clearly indicates that the measured hydrodynamic diameter is larger than the real nanoparticles dimensions (the discrepancy could be attributed to low count rate and to the strong size dependence of DLS data-fitting algorithms[41]). TEM imaging (Figure 2A; ESI S1 for additional larger images) gives a diameter of 7.0 nm (σ = 3.9 nm), 8.9 nm (σ = 4.3 nm), 8.4 nm (σ = 4.0 nm) and 8.2 nm (σ = 3.9 nm) on 4 different images from 3 different preparations (average on the four images is 8.1 nm). Moreover, XRD characterization (ESI S3) was carried out on a 5 mg sample of solid Fe_3O_4NP, obtained by addition of 100 mL acetone to 10 mL of colloidal solution, followed by decantation and drying with a N_2 flux. The reticular parameter of the sample, 8.383(±0.002) Å, corresponded to that of cubic magnetite[42]. The Fe_3O_4NP diameter determined by the Rietveld method was 10.0 nm (assuming that the Fe_3O_4NP are single crystals with no size dispersion). SEM-EDS analysis was also carried out on solid Fe_3O_4NP precipitated from their colloidal aqueous solutions (four different preparations) by acetone addition and N_2 flow drying. SEM-EDS analysis found Fe (59.7 weight %, σ = 1.4; 31.2 atomic %, σ = 0.8) and Cl (4.5 weight %, σ = 0.4; 3.7 atomic%, σ =0.4) as the only heavy elements present in the sample (H and O are the other elements present in the sample, whose % cannot be reliably determined by this technique). The Cl presence is due to the perchlorate anion adsorbed after treatment with perchloric acid in the syntethic procedure. This is also confirmed by FT-IR (ESI S4) on a solid sample of Fe_3O_4NP, showing a large band at 1070 cm^{-1} typical of the ClO_4^- anion. Thermogravimetric analysis (TGA) was also carried out (ESI S4). In a 20 °C-500 °C scan, a total weight loss of 7.3% was found, due to the release of adsorbed water and decomposition of the perchlorate anion. Finally, from the yield (61%), from the density of bulk Fe_3O_4 (5.2 g/cm^3) and from the average diameter of the Fe_3O_4NP, an average nanoparticles concentration can be calculated. Although according to TEM imaging the size distribution is large, relying on the determination of diameter by TEM the average 8.1 nm diameter was chosen for this calculation. A calculated mass of 1.45×10^{-18}g per single Fe_3O_4NP is obtained, with a 6.27×10^{-6} mol/L

concentration of Fe_3O_4NP in their colloidal solution. These values will be used in the paper for further calculations.

2. Fe_3O_4NP@MPTS. The preparation of MPTS-coated Fe_3O_4NP follows a similar approach to the syntheses described for coating iron oxides nanoparticles with SiO_2[43] using TEOS (tetraethoxysilane), based in turn on the well-established Stöber process.[44] In our approach, a given volume (1-5 mL) of the Fe_3O_4NP solution obtained as described in the previous section is diluted in a larger volume (20 mL) of ethanol. The 1:20 – 1:4 v/v dilution ratio was found optimal to a avoid aggregation during the synthetic process. Concentrated ammonia (37 %) is then added in micro additions until pH 9.5. Finally the chosen quantity of MPTS is added as pure reagent or as its ethanol solution, for high or low MPTS/Fe_3O_4NP ratios, respectively. After mechanical stirring at RT, the product is purified by centrifugation followed by redissolution in 20 mL bidistilled water. The obtained solutions are stable for a 72 h period, after which time aggregation and precipitation slowly take place. Z-potential measurement discloses in all cases weakly negative values in the -8mV – -15 mV range (this may be due both to the basic synthetic conditions leading to OH^- adsorption and to the formation of silicates on the surface as in SiO_2 nanoparticles,[45] see following discussion about vertical polimerization). ICP-OES data for Fe_{TOT} show in all cases a yield of ~ 100% with respect to the starting Fe_3O_4NP (analyses were carried out for maximum, minimum and intermediate MPTS/ Fe_3O_4NP molar ratios). A FT-IR spectrum, featuring the very weak S-H stretching band, is included in the ESI (Figure S4.4).

In our syntheses, the MPTS/Fe_3O_4NP molar ratio is made to vary from 1.1 to 7.8×10^4. A 8.1 nm spherical particle has a 2.06×10^{-12} cm^2 surface. Reactions are thus carried out with 9.7×10^{11} to 7.9×10^{16} MPTS molecules available per cm^2 of Fe_3O_4 surface. On flat silica, the maximum experimental surface concentration of MPTS is $\sim2\times10^{14}/cm^2$ grafted molecules.[40] Although in the present work the morphology and the chemical nature of the material is different, as a first approximation the used MPTS/ Fe_3O_4NP ratio ranges from a large MPTS defect to a large excess of it. DLS studies find maximum size distribution at large values (d = 50-250 nm) with no correlation with the used Fe_3O_4NP/MPTS ratio. The apparent huge dimensional increase is due to aggregation promoted by the reversible hydrophobic interactions between the MPTS coatings in aqueous solution: analysis of TEM pictures of Fe_3O_4NP@MPTS, see Figure 2B (ESI S2 for larger and additional images) disclosed separated nanoparticles and dimensions of the Fe_3O_4NP core unvaried with respect to those found for the parent Fe_3O_4NP material. Four different preparations were examined, obtaining d = 8.5 nm (σ = 4.3 nm), 9.6 nm (σ = 4.5 nm), 8.7 nm (σ = 4.8 nm) and 7.2 nm (σ = 4.5 nm) with an average of 8.5 nm. An XRD experiment (ESI S3), was carried out on samples obtained from 26000 MPTS/ Fe_3O_4NP starting ratio, revealing unchanged cubic Fe_3O_4 phase. TGA analysis was also carried out on the same sample. We found a weight loss of 12.20% in the 20-500 °C temperature range (ESI S4), with a significant increase with respect to the weight loss of nude Fe_3O_4NP, due to the MPTS coating.

Table 1 SEM-EDS analysis

MPTS / NP ratio (start)[a]	MPTS / NP ratio (end)[b]	SH[c]	Fe[d,e]		S[d,e]		Si[d,e]	
			% w	%a	% w	%a	% w	%a
7.8×10^4	25300	147	20.6 (1.4)	9.6 (0.8)	26.0 (0.1)	20.9 (0.3)	23.8 (0.2)	21.9 (0.1)
5.2×10^4	8640	114	34.9 (0.5)	16.5 (0.3)	15.0 (0.4)	12.3 (0.4)	14.59 (0.5)	13.7 (0.5)
2.6×10^4	1250	87	45.3 (1.4)	18.5 (0.9)	2.9 (0.1)	2.1 (0.2)	2.9 (0.1)	2.3 (0.2)
3.4×10^3	441	30	53.6 (4.3)	24.4 (3.3)	1.2 (0.1)	0.9 (0.1)	1.2 (0.1)	1.1 (0.1)
1	-	1	54.1 (3.2)	25.1 (2.6)	-[f]	-[f]	-[f]	-[f]

[a] molar ratio chosen in the synthesis (NP = Fe_3O_4NP); [b] molar ratio calculated from SEM-EDS % w data (NP = Fe_3O_4NP); [c] determined by colorimetric method; [d] uncertainties in parenthesis, obtained on 3 measurements of different portions of the same sample; [e] %w = weight percentage, %a = atomic percentage; [f] under the detection limits of the SEM-EDS technique;

SEM-EDS analysis detected Fe, S and Si as the only heavy elements. Weight and atomic % values are listed in Table 1 for five different preparations, ranging from the lowest to the highest used MPTS/Fe_3O_4NP ratio. S and Si atomic % have approximately the same value in all cases, as expected from functionalization with MPTS. From Fe and S weight % the total number of MPTS molecules per nanoparticles can be calculated, assuming also in this case a 8.1 nm average diameter of the Fe_3O_4NP core. As an example, values of 1250 and 441 are found for starting MPTS/Fe_3O_4NP of 26000 and 3400, respectively, with much higher values found in the preparations using a higher starting ratio, as listed in Table 1 (first and second column). Such values are also graphically visualized in Figure 3C, cyan circles, as a function of the starting MPTS/Fe_3O_4NP ratio. The very high values found for high starting ratios indicate surface functionalization taking place with simultaneous vertical and lateral polymerization of the -$Si(OCH_3)_3$ groups, forming a shell around the Fe_3O_4NP core, as sketched in Figure 1D. It has to be stressed that such a process leads to the grafting of a number of MPTS molecules whose -SH groups are not available, because hidden inside the polymer layer (sketch in Figure 3A, left). To demonstrate this, analysis of free -SH groups in Fe_3O_4NP@MPTS has been carried out by reaction with Rhodamine maleimide (RHM), see Figure 3A.

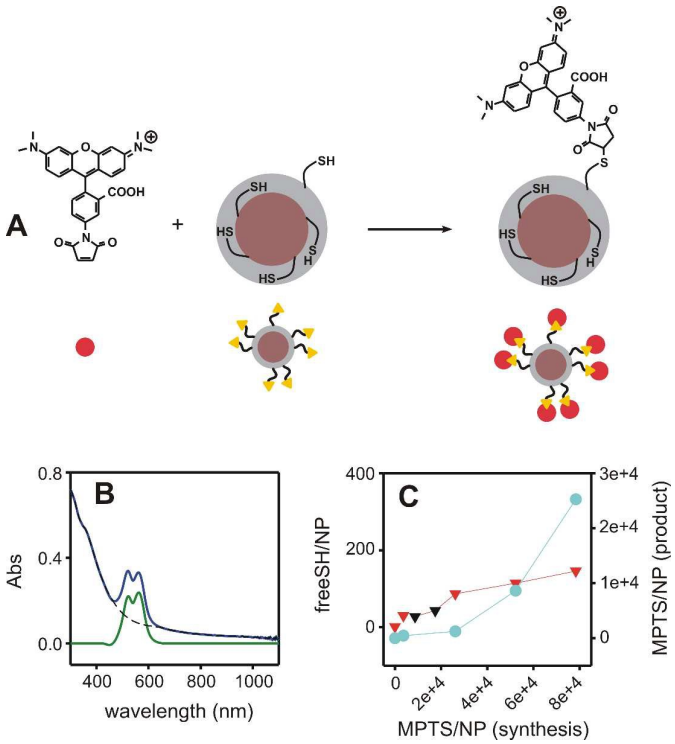

Fig 3 **A**: Schematic representation of the reaction between Fe_3O_4NP@MPTS with rhodamine maleimide. **B**: Absorption spectrum of Fe_3O_4NP@MPTS (2.6×10^4 MPTS/Fe_3O_4NP ratio in the synthesis) after reaction with rhodamine maleimide (blue solid line); calculated background absorption without rhodamine dye (black dashed line); absorption of the rhodamine moiety after background subtraction (green solid line). **C**: triangles: free –SH moieties per nanoparticles in Fe_3O_4NP@MPTS, calculated by spectrophotometry vs MPTS/ Fe_3O_4NP molar ratio in the synthesis (red points corresponds to the product analyzed with SEM-EDS in Table 1); cyan circles: MPTS molecules per Fe_3O_4NP in the product, as calculalated from SEM-EDS. Red and cyan hairlines are drawn to guide the eye

In all cases we have used a large excess of RHM with respect to the total –SH groups, as determined by SEM-EDS. The coupling reaction has ~ 100% yield,[40] so we can assume that the reactive, surface-postioned –SH groups are all functionalized with Rhodamine, as sketched in Figure 3A (right cartoon). Two cycles of ultracentrifugation, supernatant discarding and redissolution assure the full elimination of unreacted RHM. The concentration of the strongly absorbing rhodamine moiety bound to Fe_3O_4NP@MPTS is then determined by spectrophotometry. Figure 3B displays a typical spectrum on a 10-fold diluted solution (blue solid line), with the two-maximum band of RHM in the 500-600 nm range superimposing to the featureless absorption of magnetite nanoparticles. According to a published procedure,[40,46] we simulated the absorption of Fe_3O_4NP for each spectrum (black dashed line in the esample of Figure3B) as a smooth function of the wavelength, $f(\lambda) = [c1/(c2 + \lambda)] + c3$, in the range $300 < \lambda < 480$ and $600 < \lambda < 800$, i.e. out of the absorption peaks of RHM. The simulated background was subtracted to each spectrum, obtaining corrected spectra (green solid line in the example of Figure 3B). Using ε_{550} (82000 $M^{-1}cm^{-1}$ in water, pH 7) the concentration of bound RHM is obtained, corresponding to the number of available –SH groups on Fe_3O_4NP@MPTS. Figure 3C displays the obtained values as a function of the MPTS/Fe_3O_4NP ratio used in the synthesis. Only for the syntheses starting with very low MPTS/Fe_3O_4NP ratios we obtain a number of free –SH per nanoparticles corresponding to the used ratio, in correspondance to a large available surface excess on Fe_3O_4NP with respect to added MPTS. In this case, a formation of a submonolayer of MPTS on the Fe_3O_4 surface can be claimed. On increasing the MPTS/Fe_3O_4NP ratio in the synthesis, only a fraction of the added MPTS is bound to the Fe_3O_4NP surface mantaining its -SH groups available for RHM binding, see Table 1. This confirms that a larger quantity of MPTS is bound on the Fe_3O_4NP surface forming a HS-$(CH_2)_3$-Si-$(O-)_3$ polymeric shell, as it is found by SEM-EDS, Table 1, and pictorially sketched in Figure 3A. Figure 3C graphically evidences this: triangles (left vertical axis) show an increase of free -SH/ Fe_3O_4NP on increasing the MPTS/Fe_3O_4NP ratio in the synthesis, to be compared with that of cyan circles (MPTS per Fe_3O_4NP found by SEM-EDS, right vertical axis): in the latter case the increase is much steeper than in the former. This is compatible with the growth of the MPTS coating as a spherical shell around a spherical Fe_3O_4NP core: the volume of a shell, given a constant radius of the inner sphere, increases with R^3 (R= radius of the inner + shell sphere), while the surface, were free –SH are located, increases only with R^2. Moreover, part of the surface is probably occupied by $Si(O)_n^{n-}$ groups, as indicated by the negative Z-potential.

In the perspective of using Fe_3O_4NP@MPTS for further functionalization of the –SH groups, this means that our approach allows to control the number of functions that can be appended on the Fe_3O_4NP core. Due to the results obtained with GNS decoration (see below), we have chosen to use in particular the starting Fe_3O_4NP/MPTS ratio of 26000. The preparation has thus been repeated several times. The 87 free -SH value listed in Table 1 is an average value on 5 preparations, with $\sigma = 5$, this giving a good hint on the reproducibility of such approach. At this regard, the preparations with Fe_3O_4NP/MPTS ratio = 1.1 and 7.8×10^4 have been repeated 3 times each. In the first case we always obtained 1 free –SH in Fe_3O_4NP@MPTS, in the second case the 147 value listed in Table 1 is the average, with $\sigma = 6$. This indicates an effective tunability of the number of the available -SH groups per Fe_3O_4NP@MPTS, dictated by the reaction conditions. As an example of the use of the available –SH functions of Fe_3O_4NP@MPTS we have reacted such coated nanoparticles (obtained with a starting MPTS/Fe_3O_4NP ratio of 26000) with an excess of PEG_{5000}-maleimide (PEGM). PEGM is a commercial product bearing a maleimide function at one end of the PEG chain. Reaction takes place between –SH and the maleimide moiety with the same scheme described in Figure3A. The stability of obtained product, Fe_3O_4NP@MPTS-PEGM, is dramatically increased with respect to Fe_3O_4NP and Fe_3O_4NP@MPTS, as its colloidal solutions are stable for weeks and undergo repeated ultracentrifugation, supernatant discard, pellet redissolution cycles with no product lost at each cycle.

3.Magnetic characterization. The magnetic behaviour of both Fe_3O_4NP@MPTS and Fe_3O_4NP sample has been investigated by SQUID magnetometry. All the results have been normalized with respect to the total mass of each sample and are summarized in Table 2.

3.1 Fe_3O_4NP@MPTS. Figure 4 reports the magnetic data measured for a Fe_3O_4NP@MPTS sample prepared with starting MPTS/Fe_3O_4NP ratio of 26000 (87 free –SH). Panel A displays the ZFC-FC magnetization vs temperature, showing the typical behaviour expected for a sample constituted by a mono-modal size distribution of superparamagnetic particles. TEM imaging confirms such type of size distribution, although a significant standard deviation from the mean dimensional value is always found (e.g. d = 8.6nm and σ = 4.3nm in Figure S2.1-S2-3) An apparent maximum ($T_{max-(ZFC)}$) is found in the ZFC curve at 115 K.[47-49] The temperature T_{cross} (where ZFC and FC curves superpose) is 390 K. It indicates the minimum temperature where all the particles in the sample are in the superparamagnetic state. However, the difference between T_{cross} and ($T_{max-(ZFC)}$) is quite high (275 K), and could be ascribed to both large particle size distribution and/or occurrence of interparticles magnetic interactions effects. To better quantify the strength of the possible interparticles interactions, a measurement according to the TRM protocol was carried out in the same range temperature (5-400 K) as for the ZFC-FC magnetizations measurements. The magnetization measured with TRM protocol (Figure 4A, inset) decreases with the temperature increase, *i.e.* while the blocked particles are passing from the blocked state to the superparamagnetic one.

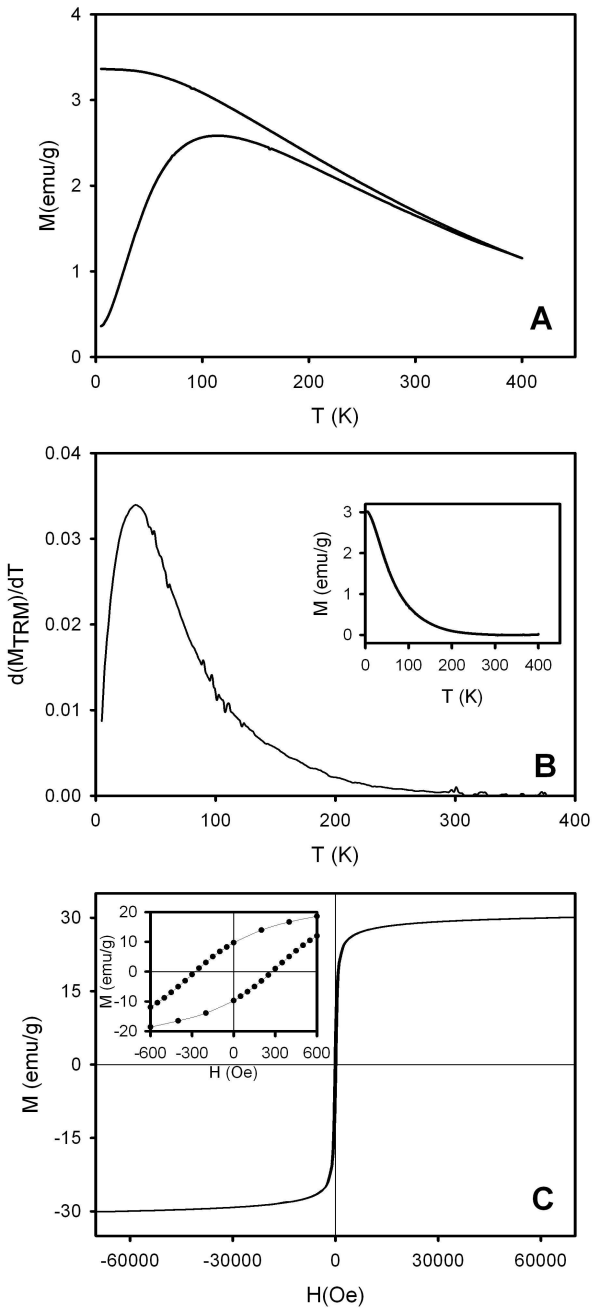

Fig 4 Magnetic data obtained for the sample Fe_3O_4NP@MPTS sample. A: ZFC-FC magnetization curves obtained by using a magnetic field of 25 Oe. B: *f(T)* function as defined by eq. 1 and obtained by the TRM reported in the inset of the panel. C: Hysteresis loop measured at T=5K, with the inset displaying the low-field range

The derivative of the TRM decay curve (Figure 4B) represents the distribution of anisotropy energy barriers[50,51]:

$$f(T) = -d(M_{TRM})/dt \quad (1)$$

Since the values of anisotropy energy barriers can be put in relation with the volume of the particles,[47] the function *f(T)* defined by eq, (1) provides then a further indirect method to determine the magnetic particles size distribution. Moreover, the TRM curve is not affected by the possible interparticle

interactions, differently from what happens in the ZFC curves, where they are established and maintained by the presence of the magnetic field under which the measurement is carried out.[52] Thus, the comparison of the $T_{max-(ZFC)}$ with the maximum of the *f(T)* curve offers a qualitative measure of the presence and strength of interparticle magnetic interactions.

Comparing the $T_{max-(ZFC)}$ value (115 K) with the maximum of the *f(T)* curve (33 K), the shift observed towards the low temperatures is equal to 82 K and is then clearly ascribable to the presence of not negligible magnetic dipolar interactions among the particles. This phenomenon is probably the cause of the low-temperature particles magnetic ordering, as indicated by the plateau that the FC magnetization reaches below about 30 K. Parameters can be extracted from the MPTS-coated sample's hysteresis loop (Figure 4C): a) the sample magnetization reaches almost complete saturation for field higher than about 50 kOe, with a relevant value of 31.1 emu/g obtained first normalizing the moment measured at 70 kOe for the sample total mass and then extrapolating it from a plot of M *versus* 1/H when H→0;[53] b) the low value of the coercive field H_C (275 Oe) is in agreement with that expected for a soft magnetic materials such as magnetite; c) the reduced remnant magnetization M_R/M_S (0.31) is lower than 0.5, being the latter the value reported in the Stoner-Wohlfart theory[54] as the expected one in the case of an ensemble of non-interacting blocked particles with uniaxial anisotropy. Such a lowering is a well-known effect of the presence of magnetic interactions among the particles, further confirming what already observed also by ZFC-FC and TRM curves (see alsto Table S5, ESI, for summarized data).

3.2 Fe_3O_4NP. Figure S5 (ESI) reports the magnetic data measured for the Fe_3O_4NP sample. Analogously to that reported in Figure 4, panel A shows the ZFC-FC magnetizations *vs* temperature. However, differently from what observed for Fe_3O_4NP@MPTS, the ZFC-FC curves show a a superparamagnetic behaviour but with the ZFC displaying now three maxima ($T_{max-(ZFC)}$) at 197, 268 and 325 K. T_{cross} is out of the explored thermal range, *i.e.* higher than 400K, indicating that even at that temperature a fraction of the magnetic particles is still in the blocked state, as probable results of large particle size distribution and/or occurrence of strong interparticles magnetic interactions. The three maxima in the ZFC magnetization could be explained by a three-mode particle size distribution, but this is in contrast with TEM imaging, displaying a mono-modal particle size distribution (although with a significant standard deviation affecting the average value, see ESI, Figure S2.1-S2.12). A TRM measurement was then carried out (ESI, panel B, Figure S5). Comparing the $T_{max-(ZFC)}$ values with those observed in the *f(T)* curve, only the first one of *f(T)* at 55K is shifted towards low temperatures with respect to the first maximum observed in the ZFC curve (197 K). Their difference is 142 K, much higher than that observed for the MPTS-coated sample, thus ascribable to much stronger magnetic interactions between uncoated particles. On the other hand, the two further maxima observed in *f(T)* curve (at 266 and 300 K) are very close to those observed in the ZFC curves (268 and 315 K)a manifestation of a double transition to collective ordering occurring at those temperatures, due to the very strong interactions among the particles. These collective magnetic orderings are then destroyed by the further temperature increase. The strong tendency to give rise to particles collective magnetic ordering still at high temperature is further clearly confirmed by the plateau that the FC curve reaches at about 310 K, a much higher temperature than the one observed for the MPTS-coated sample. Finally, also the parameters extracted from the Fe_3O_4NP isothermal hysteresis loop (ESI, Figure S5C), confirm the occurrence of much stronger interactions with respect to Fe_3O_4NP@MPTS (ESI S5 and Table S5 for details).

4. GNS decoration. The GNS used in this research were prepared according to a well-established synthesis developed in our group,[30,31] with a seed growth approach that uses LSB as the directing and protecting agent. In the used conditions (see Experimental) we obtain GNS as a mixture of monocrystalline 4-branched objects (~ 30 %) and of larger pentatwinned objects (70%) featuring from 2 to 5 branches (average = 3). The LSPR of the first species has a maximum at 630-650 nm and that of the second species in the 850-900 nm range. This mixture produces the typical two-maximum absorption spectrum of the GNS colloidal solutions, as shown in ESI (Figure S6.1, black solid line; the low absorption maximum at 520 nm is due both to some spherical by-products and to the transversal oscillation of the valence electrons in the branches). As we have already shown,[33] both typologies has the same average mass (5×10^{-17}g/GNS). Their molar concentration can thus be calculated from the Au concentration determined by ICP-OES after the growth process and a ultracentrifugation-redissolution cycle. In this case we obtained Au = 0.0591 g/L and [GNS] = 1.96×10^{-9} M. Interaction of the GNS surface with thiolated molecules typically results in a LSPR shift of 5-30 nm, due to the change in the local refractive index and depending on the nature of the added thiol.[33,34]

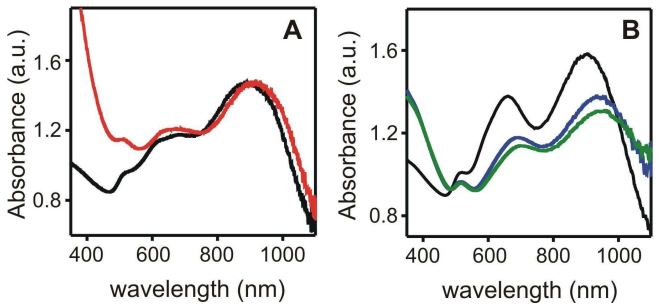

Fig 5 A: Absorption spectrum of GNS solution (black solid line) and of the GNS after the addition of 120 μL of Fe_3O_4NP@MPTS solution ('87 SH') corresponding to a 20-fold molar excess of Fe3O4NP@MPTS (red solid line). **B**: Absorption spectrum of GNS solution (black solid line) and of the GNS after the addition of 120 μL of 'nude' Fe_3O_4NP corresponding to a 20-fold molar excess of Fe3O4NP@MPTS. Blue: after 10 minutes. Green: after 80 minutes. Spectra have been normalized at 486 nm, the original blue and green spectra showed higher Abs values due to the featureless absorption/scattering of turbidity. The starting spectra (black) slightly differs between A and B as they were taken on two different GNS preparations

We treated the GNS solution with three typologies of Fe_3O_4NP@MPTS, i.e. coated with 147, 87 and 1 available -SH. In all cases we added 20 μL portions (1.25×10^{-10} mol) of the Fe_3O_4NP@MPTS solutions to 10 mL (1.96×10^{-11} mol) of the GNS solution. In the case of Fe_3O_4NP@MPTS with 1 available -SH groups, no variation was observed in the GNS absorption spectrum. In the case of the same nanoparticles with 87 available -SH groups the longer LSPR progressively red shifted with a maximum $\Delta\lambda$ = 10 nm after 120 μL addition, corresponding to a ~ 40-fold molar excess of Fe_3O_4NP@MPTS vs GNS, Figure 5A, red solid line.

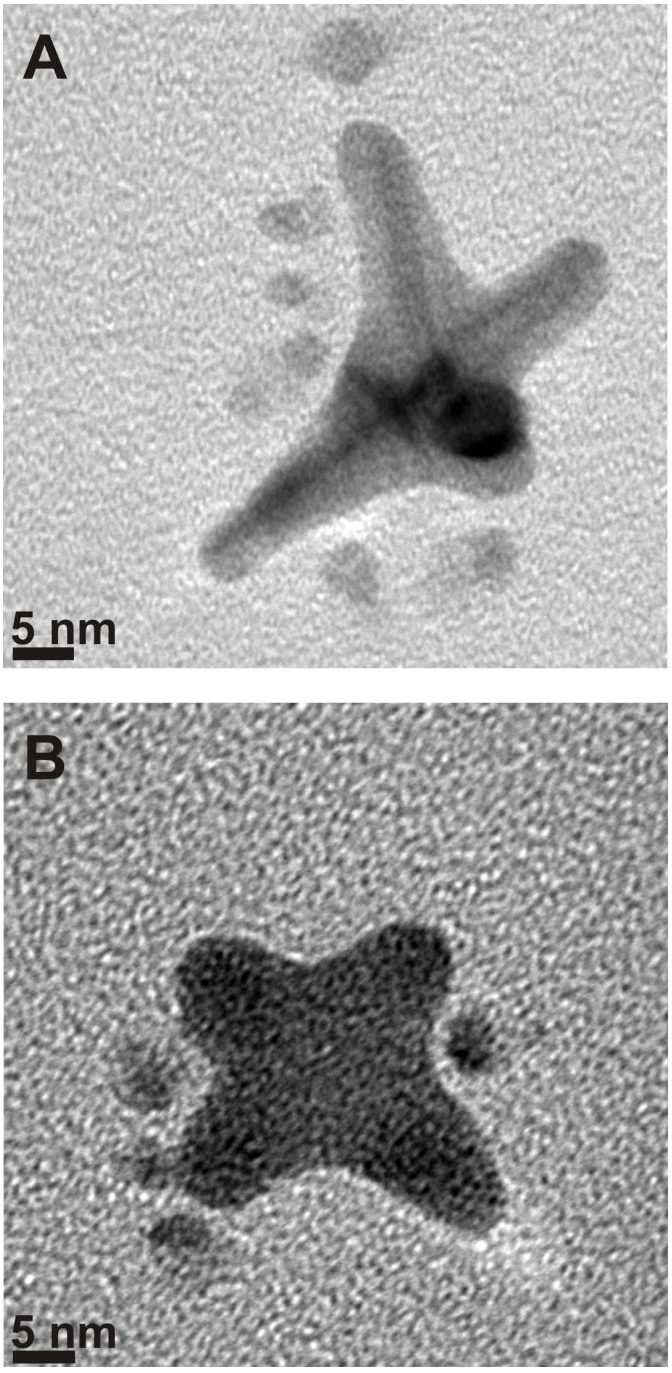

Fig 6 A: Fe_3O_4NP@MPTS decorating GNS of the pentatwinned typology. B: same, with monocrystalline, 4-branched GNS

Addition of Fe_3O_4NP@MPTS with 147 –SH resulted in the very quick (< 5 min) precipitation of the mixture. It has to be noticed that both GNS and Fe_3O_4NP@MPTS have negative Z-potential. The results suggest that electrostatic repulsion holds, unless a large number of binding sites is available on the Fe_3O_4NP@MPTS surface, as in the case of nanoparticles with 87 -SH. However, further increasing in the number of free -SH also leads to the exponential increase of the MPTS polymerized layer (see Table 1 and Figure 3C) and of the Fe_3O_4NP@MPTS overall dimensions, producing large, unstable hybrids when interacting with GNS, as in the case of the "147 –SH" nanoparticles. We also treated GNS with 120 μL of the solution of Fe_3O_4NP (same molar ratio as before). These have Z-potential = + 28mV and in this case, electrostatic attraction drives interaction, resulting in a large LSPR red shift, with $\Delta\lambda$ = +30 nm, see Figure 6B, blue and green solid lines. However, also in this case fast precipitation takes place (within 2 hours), probably due to the bridging of positive Fe_3O_4NP between negatively charged GNS. Positively charged Fe_3O_4NP were also enveloped in a layer of the anionic polymer PSS (sodium polystyrene sulphonate) by addition of excess PSS and purification by ultracentrifugation, supernatant discard and pellet redissolution in bidistilled water. The obtained negatively charged Fe_3O_4NP@PSS (Z potential = - 32 mV) were added to the GNS solution in the same concentration as Fe_3O_4NP@MPTS and Fe_3O_4NP. In this case, no spectral variation was observed, in agreement with a repulsive electrostatic interaction. As a final control to exclude the role of any free unreacted MPTS surviving the ultracentrifugation purification procedures in the Fe_3O_4NP@MPTS synthesis, we added also pure MPTS to a GNS solution. We used the same total concentration as after the addition of 120 μL of "87 –SH" Fe_3O_4NP@MPTS, observing a dramatically different behaviour with the respect to the addition of the "87 –SH" coated magnetite nanoparticles, i.e. a +15 nm LSPR shift followed by slow precipitation see ESI, Figure S6.

Following the indications obtained from the interaction experiments, TEM images were recorded by dropcasting solutions of GNS decorated with Fe_3O_4NP@MPTS featuring 87 free -SH. Under our experimental conditions, TEM allowed enough contrast to distinctly identify GNS and Fe_3O_4NP, while the MPTS layer appeared transparent. This result can be explain considering the difference in electron-density between gold, iron oxide and MPTS, and the vertical polymerisation model discussed above, leading to a considerably low electron-density shell around the Fe_3O_4NPs. Figure 6 displays two representative images, showing decorated GNS of the pentatwinned type (A) and of the monocrystalline type (B). In both cases, Fe_3O_4NP@MPTS adhere to the surface of GNS with apparent inter-particle gaps between 1 and 2 nm, consistent with a MPTS layer formed with partial vertical polymerization, as hypothesized in the previous sections (more images are available in the ESI, S7).

Conclusions

We have demonstrated that magnetite nanoparticles can be coated with a tunable quantity of MPTS, thanks to the control of a simple parameter such as the MPTS/Fe_3O_4NP ratio in the coating steps. The added MPTS forms a shell around the Fe_3O_4NP core by vertical and lateral polymerization, so that at high MPTS/Fe_3O_4NP ratios only a part of the –SH groups are available for further functionalization, the majority being hidden in the shell. However, the number of such available surface –SH (counted by a colorimetric method) is also tunable, allowing to know how many free –SH can be obtained per single Fe_3O_4NP under given synthetic conditions. This in turn could allow further studies on mixed functionalization, by using different molecules featuring groups that react in high yield with thiols (eg maleimide) and tuning their stoichiometry. Moreover, MPTS coating significantly reduces the magnetic interactions occurring between the magnetite cores, effectively preventing the occurrence of collective magnetic states and providing the typical behaviour of superparamagnetic nanoparticles. Provided that a good balance is used between the number of available –SH and the overall size of Fe_3O_4NP@MPTS, such nanoparticles interact with GNS decorating their surface, thus leading to potential theranostic hybrids, featuring both the superparamagnetic properties of small magnetite nanoparticles, added to the magnetothermal properties of the latter, and to the plasmonic and optical photothermal properties of GNS.

Acknowledgements

We thank Fondazione Cariplo Milano, Italy (project 2010-0454), MIUR (PRIN 2010-2011, 20109P1MH2_003) and the University of Pavia (Fondo Ricerca Giovani) for funding.

Notes and references

[a]Dipartimento di Chimica, Università di Pavia, viale Taramelli, 12 - 27100 Pavia, Italy;
[b]King Abdullah University of Science and Technology (KAUST), Biological and Environmental Sciences and Egineering Division (BESE), 23955-6900 Thuwal, Kingdom of Saudi Arabia
[c]Department of Chemistry, ~~Università~~ University of Liverpool, Crown Street, Liverpool L69 7ZD, United Kingdom;
[d]Dipartimento di Chimica, Università di Parma, Parco Area delle Scienze, 17/A 43124 Parma, Italy
E-mail: piersandro.pallavicini@unipv.it; Fax (+39)0382 528 544; Tel (+39) 0382 987 336

Electronic supplementary information (ESI) available: See DOI: 10.1039/b000000x/

1 - R. Weissleder, A. Bogdanov, E.A. Neuwelt, and M. Papisov *Adv. Drug Del. Rev.*, 1995, **16**, 321
2 - S.K. Yen, P. Padmanabhan and S.T. Selvan, *Theranostics,* 2013, **3**, 986
3 - J. He, M. Huang, D. Wang, Z. Zhang and G. Li, *J. Pharmaceut. Biomed.*, 2014, **101**, 84
4 - A. Jordan, R. Scholz, P. Wust, H. Schirra, T. Schiestel, H. Schmidt and R. Felix, *J. Mag. Mag. Mater.*, 1999, **194**,185
5 - L. Sironi, S. Freddi, M. Caccia, P. Pozzi, L. Rossetti, P. Pallavicini, A. Donà, E. Cabrini, M. Gualtieri, I. Rivolta, A. Panariti, L. D'Alfonso, M. Collini and G. Chirico, *J. Phys. Chem. C*, 2012, **116**, 18407
6 - Y. Sahoo, A. Goodarzi, M.T. Swihart, T.Y. Ohulchanskyy, E.P. Furlani, and P.N. Prasad, *J. Phys. Chem. B*, 2005, **109**, 3879
7 - D. K. Kim, M. Mikhaylova, Y. Zhang, and M. Muhammed, *Chem. Mater.*, 2003, **15**, 1617
8 - H. Benbenishty-Shamir, R. Gilert, I. Gotman, E. Y. Gutmanas, and C.N. Sukenik, *Langmuir*, 2011, **27**, 12082
9 - T.J. Daou, G. Pourroy, J.M. Greneche, A. Bertin, D. Felder-Flesch, and S. Begin-Colin, *Dalton Trans.*, 2009, **23**, 4442
10 - T.J. Daou, J.M. Greneche, G. Pourroy, S. Buathong, A. Derory, C. Ulhaq-Bouillet, B. Donnio, D. Guillon and S. Begin-Colin, *Chem. Mater.*, 2008, **20**, 5869
11- M. Di Marco, C. Sadun, M. Port, I. Guilbert, P. Couvreur, and C. Dubernet, *Int. J. Nanomed.*, 2007, **2**, 609
12 - P. Pallavicini, G. Dacarro, Y.A. Diaz-Fernandez, and A. Taglietti, *Coord. Chem. Rev.*, 2014, **275**, 37
13 - D. Li, W.Y. Teoh, J.J. Gooding, C. Selomulya, and R. Amal, *Adv. Funct. Mater.* 2010, **20**, 1767
14- R. P. Pogorilyi, I. V. Melnyk, Y. L. Zub, G. A. Seisenbaeva and V. G. Kessler, *J. Mater. Chem. B*, 2014, **2**, 2694
15 - X. Shen, X. Fang, Y. Zhou, and H. Liang, *Chem. Lett.*, 2004, **33**, 1468
16 - M. Ma, Y. Zhang, W. Yu, H. Shen, H. Zhang, and N. Gu, *Colloid Surf. A*, 2003, **212**, 219
17 - I. J. Bruce and T. Sen, *Langmuir*, 2005, **21**, 7029.
18 - A. del Campo, T. Sen, J.-P. Lellouche, and I. J. Bruce, *J. Magn. Magn. Mater.,* 2005, **293**, 33
19 - B. Yoza, M. Matsumoto and T. Matsunaga, *J. Biotechnol.*, 2002, **94**, 217.
20 - P. Ashtari, X. He, K. Wang and P. Gong, *Talanta*, 2005, **67**, 548
21 - M. T. Dulay, Q. J. Baca and R. N. Zare, *Anal. Chem.* 2005, **77**, 4604
22 - I. Koh, X. Wang, B. Varughese, L. Isaacs, S. H. Ehrman and D. S. English, *J.Phys. Chem. B,* 2006, **110**, 1553.
23 - N. R. Jana, C. Earhart and J. Y. Ying, *Chem. Mater.*, 2007, **19**, 5074
24 - Z. Skeete, H. Cheng, E. Crew, L. Lin, W. Zhao, P. Joseph, S. Shan, H. Cronk, J. Luo, Y. Li, Q. Zhang, and C.-J. Zhong, *ACS Appl. Mater. Interfaces*, 2014, **6**, 21752
25 - T.-D. Nguyen and T.-H. Tran, *RSC Adv.*, 2014, **4**, 916
26 - H.-Y. Park, M. J. Schadt, L. Wang, I-Im S. Lim, P. N. Njoki, S. H. Kim, M.-Y. Jang, J. Luo, and C.-J. Zhong, *Langmuir*, 2007, **23**, 9050
27 - X. Shen, Z. Ge,and Y. Pang, *J. Solid State Chem.*, 2015, **222**, 37
28 - W.-C. Huang, P.-J. Tsai, and Y.-C. Chen, *Small*, 2009, **5**, 51
29 - C. Wang and J. Irudayaraj, *Small*, 2010, **6**, 283
30 - P. Pallavicini, G. Chirico, M. Collini, G. Dacarro, A. Donà, L. D'Alfonso, A. Falqui, Y. A. Diaz-Fernandez, S. Freddi, B. Garofalo, A. Genovese, L. Sironi and A. Taglietti, *Chem. Commun.*, 2011, **47**, 1315
31 - A. Casu, E. Cabrini, A. Donà, A. Falqui, Y. Diaz-Fernandez, C. Milanese, A. Taglietti and P. Pallavicini, *Chemistry Eur J.*, 2012, **18**, 9381
32 - P. Pallavicini, A. Donà, A. Casu, G. Chirico, M. Collini, G. Dacarro, A. Falqui, C. Milanese, L. Sironi, and A. Taglietti, *Chem. Commun.*, 2013, **49**, 6265

33 - P. Pallavicini, C. Bernhard, G. Chirico, G. Dacarro, F.Denat, A. Donà, C. Milanese and Angelo Taglietti, *Dalton Trans.*, 2015, **44**, 5652
34 - P. Pallavicini, E. Cabrini, G. Cavallaro, G. Chirico, M. Collini, L. D'Alfonso, G. Dacarro, A. Donà, N. Marchesi, C. Milanese, A. Pascale, L. Sironi, A. Taglietti, *J. Inorg. Biochem.*, 2015, *in the press, doi:10.1016/j.jinorgbio.2015.05.002*
35 - S. Freddi, L. Sironi, R. D'Antuono, D. Morone, A. Donà, E. Cabrini, L. D'Alfonso, M. Collini, P. Pallavicini, G. Baldi, D. Maggioni, and G. Chirico, *Nano Letters*, 2013, **13**, 2004−2010
36 - P. Pallavicini, A. Donà, A. Taglietti, P. Minzioni,M. Patrini, G. Dacarro, G. Chirico, L. Sironi, N. Bloise, L. Visai and L. Scarabelli, *Chem. Commun.*, 2014, **50**, 1969
37 - G. Chirico, M. Collini, and P. Pallavicini, *Nanomedicine*, 2014, **9**, 1
38 - P. Pallavicini, S. Basile, G. Chirico, G. Dacarro, L. D'Alfonso, A. Donà, M. Patrini, A. Falqui, L. Sironi, and A. Taglietti, *Chem. Commun.*, 2015, **51**, 12928
39 - R. Massart, *IEEE Trans. Magn.*, 1981, **17**, 1247-1248
40 - P. Pallavicini, G. Dacarro, M. Galli, M. Patrini, *J. Colloid Interf. Sci.*, 2009, **332**, 432
41 - Y. A. Diaz-Fernandez, P. Pallavicini, L. Pasotti, C. Milanese, E. Pellicer, M. D. Barò, Y. Rend, and L. Malavasi, *Nanoscale*, 2011, **3**, 4220
42 - JCPDS crystallographic card n° 00-019-0629
43 - Y. Lu, Y. Yin, B. T. Mayers and Y. Xia, *Nano Letters*, 2002, **2**, 183-186
44 - W. Stöber, A. Fink, and E. Bohn, *J. Colloid Interface Sci.*, 1968, **26**, 62
45 - A. Lamberty, K. Franks, A. Braun, V. Kestens, G. Roebben, and T. P. J. Linsinger, *J. Nanopart. Res.*, 2011, **13**, 7317
46 - A.V. Krasnoslobodtsev, and S.N. Smirnov, *Langmuir* 2002, **18**, 3181
47 - L. Néel, *Ann. Geophys.*, 1949, **5**, 99.
48 - M. Respaud, J. M. Broto, H. Rakoto, A. R. Fert, L. Thomas, B. Barbara, M. Verelst, E. Snoeck, P. Lecante, A. Mosset, J. Osuna, T. Ould Ely, C. Amiens and B. Chaudret, *Phys. Rev. B: Condens. Matter Mater. Phys.*, 1998, **57**, 2925.
49 - A. Casu, M.F. Casula, A. Corrias, A. Falqui, D. Loche, S. Marras and C. Sangregorio, *Phys. Chem. Chem. Phys.*, 2008, **10**, 1043.
50 - A.J. Rondinone, A.C.S. Samia, and Z.J. Zhang, *J. Phys. Chem. B*, 1999, **103**, 6876.
51 - A. Casu, M.F. Casula, A. Corrias, A. Falqui, D. Loche and S. Marras, *J. Phys. Chem. C*, 2007, **111**, 916.
52 - R.W. Chantrell, M. El-Hilo, and K. O'Grady, *IEEE Trans. Magn.*, 1991, **27**, 3570.
53 - S. R. Ahmed, S. B. Ogale, G. C. Papaefthymiou, R. Ramesh and P. Kofinas, *Appl. Phys. Lett.*, 2002, **80**, 1616.
54 - E.C. Stoner, and E.P. Wohlfart, *IEEE Trans. Magn.*, 1991, **27**, 3475

Superparamagnetic magnetite nanoparticles are coated with a tunable number of free surface –SH, enabling them to decorate gold nanostars